A Reduced-Order Generalized Proportional Integral Observer-Based Resonant Super-Twisting Sliding Mode Control for Grid-Connected Power Converters

Lu, Jinghang; Savaghebi, Mehdi; Ghias, Amer M.Y.M.; Hou, Xiaochao; Guerrero, Josep M.

Published in:
IEEE Transactions on Industrial Electronics

DOI (link to publication from Publisher):
10.1109/TIE.2020.2998745

Publication date:
2021

Document Version
Accepted author manuscript, peer reviewed version

A Reduced-Order Generalized Proportional Integral Observer-based Resonant Super-twisting Sliding Mode Control for Grid-Connected Power Converters

Jinghang Lu,*Member, IEEE*, Mehdi Savaghebi, *Senior Member, IEEE, Membership,* Amer M.Y.M Ghias, *Member, IEEE,* Xiaochao Hou*, Student Member IEEE,* Josep M Guerrero, *Fellow, IEEE*

***Abstract*—This paper presents a reduced-order generalized proportional-integral observer (RGPIO) based resonant super-twisting sliding mode controller (RST-SMC) for the three-phase AC/DC converters. On the contrary to utilizing the proportional-integral (PI) controller in regulating the DC-link voltage, which may cause large undershoot/overshoot under the disturbance, the proposed voltage control strategy for the DC-link has high disturbance rejection ability and the settling time has been greatly reduced. In addition, the proposed RST-SMC in the current control loop not only preserve the merits of the sliding mode controller but also achieve the current tracking without steady-state error in the stationary $\alpha-\beta$ frame. The effectiveness of the proposed method has been verified by a lab-constructed experimental prototype.**

***Index Terms*—Disturbance Rejection; Reduced-order generalized proportional-integral observer; Sliding mode control; Three-phase converter;**

I. INTRODUCTION

Last few years have witnessed the wide implementation of the grid-connected converters in various industrial areas, such as the front stage of on-line uninterruptible power supply (UPS) system, hybrid AC/DC microgrid, railway electrification systems, etc. [1-5]. In order to achieve stable and efficient operation of the three-phase grid-connected converter, various control strategies have been applied in this system [6, 7]. Typically, an outer voltage loop and an inner current loop are constructed in the control system, and the linear regulators, such as PI controllers, are adopted in the voltage and current loop control system [6]. However, the main disadvantage of this approach is that the system's performance is limited by the PI parameters, which cause the dynamic response under disturbance to be quite slow. A faster response can be improved by applying a deadbeat control strategy, but it is well known to be highly sensitive to parameter uncertainty. Alternatively, several nonlinear control strategies have been proposed for the AC/DC converter, such as passivity-based control strategy [8], model predictive control [9]， and sliding mode control (SMC) [10-12]. Among these control strategies, the SMC has attracted great attention due to its fast dynamic response, high robustness against uncertainties and satisfactory performance in a wide range of operating conditions [13, 14]. In recent years, different SMC strategies have been proposed for grid-connected power converters. Among these strategies, integral SMC and equivalent control are two popular examples of such methods [15-17]. In [18, 19], the hysteresis modulation based SMC control strategy for the LCL type converter are proposed. In [20] a model predictive based sliding mode control is proposed for the AC/DC converters. These methods, however, suffer from the chattering issue, which causes high-order harmonics in the converter output current [21]. In order to suppress the chattering issue and regulate the AC signal, reference, [22] proposed a multi-resonant sliding surface (MRSS) based control strategy to suppress the current reference tracking error. However, this SMC comprises of multiple sliding surfaces, which is too complicated to be implemented. Besides, the large computation of MRSS inevitably impedes the application in low-cost controllers.

To deal with the aforementioned chattering issue and reduce the computation burden, the application of the super-twisting theory in SMC design has been proposed recently. The super-twisting SMC enjoys all the merits of the SMC without being affected by the chattering issue [23-27]. Traditional super-

Manuscript received November 29, 2019; revised March 13, 2020; April 21,2020 and May 6,2020 accepted May 14, 2020. (*Corresponding author: Jinghang Lu*)

Jinghang Lu is with with school of mechanical engineering and automation, Harbin Institute of Technology (Shenzhen), Shenzhen, China (Jinghang.lu@ieee.org),

M. Savaghebi is with Electrical Engineering Section, the Mads Clausen Institute, University of Southern Denmark, Odense, Denmark (email: mesa@mci.sdu.dk)

Amer M.Y.M. Ghias is with School of Electrical and Electronic Engineering, Nanyang Technological University, Singapore, 639798 (email: amer.ghias@ntu.edu.sg)

Xiaochao Hou is with School of Automation, Central South University, Changsha, 410083 China.(email: houxc10@csu.edu.cn)

Josep M.Guerrero is with the Department of Energy Technology, Aalborg University, Aalborg DK-9220, Denmark. (email: joz@et.aau.dk)

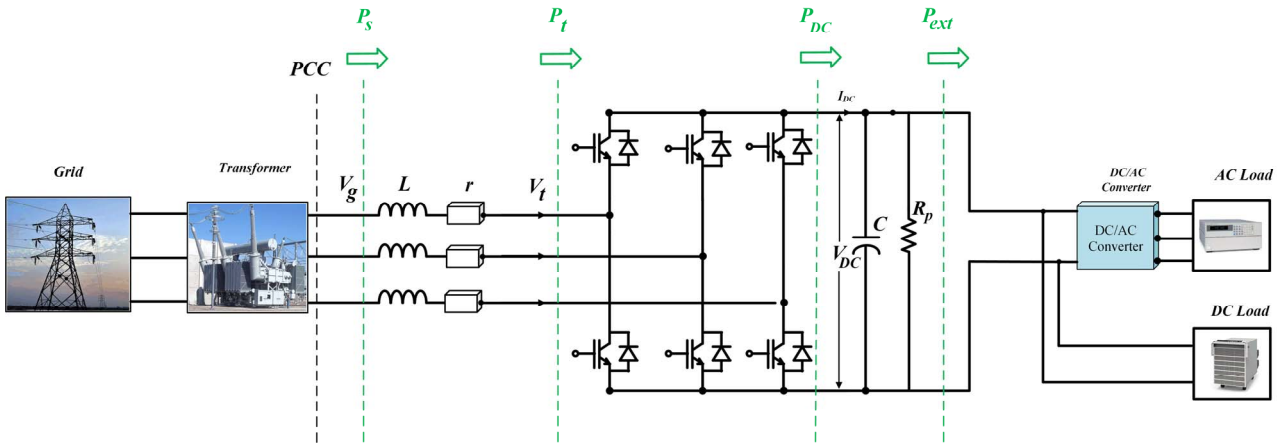

Fig.1. Configuration of a grid-connected power converter

twisting SMC, nevertheless, can only regulate the current in the *d-q* frame [12, 28, 29], which means this method cannot guarantee a zero steady-state error tracking in $\alpha-\beta$ frame , hence, an enhanced ST-SMC needs to be investigated to realize the ST-SMC to be working in tracking the AC signal while preserving the merits of ST-SMC. In addition, in the previous works, the PI controllers are normally adopted for controlling the DC-link capacitor's voltage of the three-phase AC/DC converter. However, the PI parameters can hardly be tuned automatically under the load disturbances. In order to enhance the dynamic response of the DC-link voltage under the various disturbances, a DC-link current sensor is installed, and the feedforward control strategy has been added to the DC-link control [30]. However, this method may not be desirable from the reliability point of view, and the uncertainty of the system can not be measured with this method. To deal with this issue, several advanced control strategies have been designed to improve the DC-link dynamics with the sensor-less control structure. In [31], a nonlinear disturbance observer is proposed. It shows good performance at the expense of complicated analysis and tuning of the parameter. In [32, 33], a set of H-infinity controller and an adaptive control strategy are adopted for the DC-link voltage and current loops, the simulation results show good dynamic performance. In [34], a singular-value synthesis control strategy is proposed for the DC-link voltage regulation. However, the design guide is based on the worst scenario, which may degrade the controller's performance at the normal working condition. Recently, an enhanced state observer (ESO) has been proposed to actively compensate for the disturbance and the system's uncertainty. However, the ESO is only applicable for the constant or slow varying disturbance estimation [35]. Unlike ESO, the GPIO can estimate various disturbances if these disturbances can be described in time-dependent terms，and it has been successfully applied in the DC-DC converter control and motor drive [36, 37]. In [37], the optimized GPIO is designed to estimate the disturbance and system uncertainties for the DC-DC circuit. [38, 39] propose the current predictive control with augmented GPIO to suppress the ripple in permanent magnet linear synchronous machine. In addition, the backstepping control combined with the GPIO has been proposed for the diesel engine to improve the dynamic performance and disturbance rejection ability [40]. But this method has not been applied in the DC-link voltage disturbance rejection in the three-phase AC/DC converter.

In this paper, aiming to improve the system performance with outer voltage loop under load disturbances and the parameter uncertainty, and also to achieve the fast and robust inner current loop regulation, a reduced-order GPIO (RGPIO) based resonant ST-SMC (RST-SMC) method is developed. Specifically, the proposed controller has a cascaded structure that consists of two control loops. The outer loop adopts an RGPIO based proportional control to regulate the DC-link voltage, while the inner loop adopts an RST-SMC controller to regulate the converter's current. The contribution of this paper is summarized as follows:

First, for the outer DC-link voltage regulation loop, the load connection/disconnection causes the disturbance, which may affect the system's dynamic performance. In addition, the load change may cause system parameter variation. In order to conquer these issues, an RGPIO is proposed to actively estimate and cancel the disturbance and parameter uncertainty in real-time. In addition, a proportional DC-link voltage regulator is able to achieve voltage reference tracking without steady-state error by incorporating RGPIO.

Second, an RST-SMC strategy is proposed for the inner loop current regulation. With the proposed control strategy, the zero steady-state current tracking capability is ensured, and a fast dynamic response is achieved in the $\alpha-\beta$ frame. Moreover, the proposed controller also offers a high disturbance rejection capability, which leads to a low THD current.

Finally, the proposed control strategies are verified with experimental tests, which demonstrate good dynamic performance and a wide robustness range with load disturbance.

This paper is unfolded as follows: Section II outlines the system configuration and modeling of the three-phase AC/DC converter. The RGPIO based DC-link voltage control strategy is designed and discussed in Section III. The RST-SMC based

inner loop control strategy is presented in Section IV. The simulation results are provided in Section V. The experimental comparative results are illustrated in Section VI. Finally, the conclusions are drawn in Section VII.

II. MODELING OF THE AC/DC CONVERTER

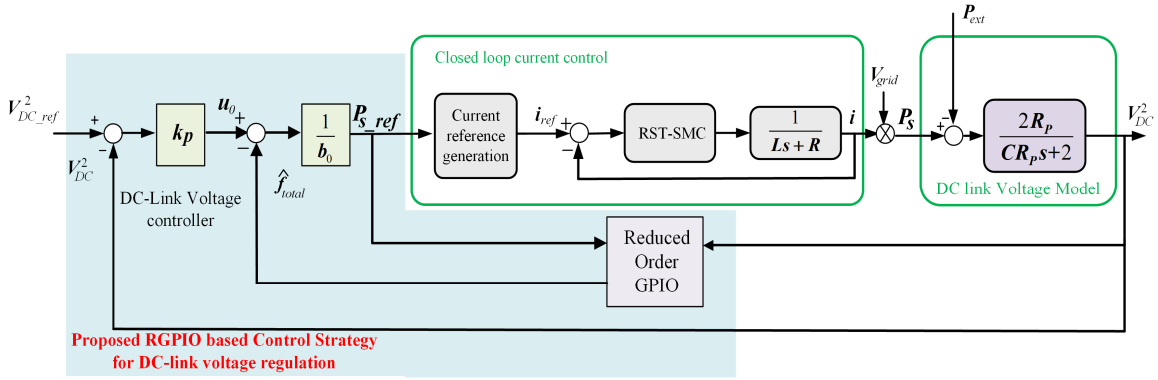

Fig.2. Reduced-order GPIO based block diagram of the dual-loop control structure for the three-phase AC/DC converter

A typical grid-connected power converter system is shown in Fig.1, where a three-phase AC/DC converter is adopted as the interface between the grid and the load. As is shown in Fig.1, the L-type filter is adopted as the output filter of the converter, r is the parasitic resistance of the filter, V_{DC} is the DC-link voltage. V_t is the output voltage of the inverter, V_g is the grid voltage at Point of Common Coupling (PCC). By assuming a balanced grid voltage, the system model in $\alpha-\beta$ reference frame is expressed as:

$$L\frac{di_\alpha(t)}{dt}+ri_\alpha(t)=V_{g\alpha}(t)-V_{t\alpha}(t) \tag{1a}$$

$$L\frac{di_\beta(t)}{dt}+ri_\beta(t)=V_{g\beta}(t)-V_{t\beta}(t) \tag{1b}$$

where $V_{g\alpha}$ and $V_{g\beta}$ indicate the grid voltage in the $\alpha-\beta$ reference frame, $V_{t\alpha}$ and $V_{t\beta}$ are the output voltage of the converter, i_α and i_β are the output current in the $\alpha-\beta$ reference frame, respectively.

The DC-link voltage controller is responsible for keeping the DC-link voltage to be constant by balancing the injected power and the output active power of the DC-link. Hence, the power balance across the DC-link capacitors in Fig.1 is expressed as:

$$\frac{d}{dt}(0.5CV_{DC}^2)=P_{DC}-P_{ext}-P_{loss}=P_t-P_{ext}-P_{loss} \tag{2}$$

where V_{DC} is the DC link voltage, C is the DC link capacitance, $P_{DC}=V_{DC}I_{DC}$, which is equal to the rectifier ac-side terminal power P_t, P_{ext} is the external power that flows out of the DC capacitor. P_{loss} is the power loss in the converter circuit and expressed as: $P_{loss}=\frac{V_{DC}^2}{R_p}$, R_p represent the total switching loss of the system. Eq.(2) stands for the instantaneous power balance between the dc side and the ac side of the three-phase AC/DC converter, on the left side of the Eq.(2), meanwhile, in the right side of (2). By neglecting the instantaneous power of the AC side filter, the AC side terminal power P_t is equal to the grid side power P_s. Therefore, by considering this fact, (1) can be expressed as:

$$\frac{d}{dt}(0.5CV_{DC}^2)=P_s-P_{ext}-\frac{V_{DC}^2}{R_p} \tag{3}$$

III. THE OUTER LOOP RGPIO BASED DC-LINK VOLTAGE CONTROLLER DESIGN

A. The design of RGPIO

In this section, A RGPIO is designed for observing and actively canceling the lumped disturbance caused by the external disturbance and internal system parameter variation.

By taking the Laplace transfer function of both sides of (3), The expression can be derived as:

$$V_{DC}^2(s)=\frac{2R_p}{CR_ps+2}P_s(s)-\frac{2R_p}{CR_ps+2}P_{ext}(s) \tag{4}$$

where V_{DC}^2 and P_s are the system state and control input, respectively, and $P_{ext}(s)$ is the system's disturbance input.

By re-arranging (2), the following expression is derived as:

$$\frac{d}{dt}V_{DC}^2=\frac{2}{C}P_s-\frac{2}{C}\left(P_{ext}+\frac{V_{DC}^2}{R_p}\right)=\frac{2}{C}P_s+f_{total} \tag{5}$$

where f_{total} denotes the lumped disturbance, including the external disturbance $(-\frac{2}{C}P_{ext})$ and the capacitance uncertainty $(-\frac{2}{C}\frac{V_{DC}^2}{R_p})$ and other unmodeled disturbance, such as EMI of the DC-link capacitance. It should be noted that these disturbances cannot be directly observed by the traditional PI controller or the Luenberger observer; on the contrary, in the following, these disturbances will be modeled by the proposed RGPIO.

In the full-order GPIO design, the state space modeling of the DC-link is expressed as:

$$\begin{bmatrix}\dot{x}_1\\ \dot{x}_2\\ \dot{x}_3\end{bmatrix}=\begin{bmatrix}0&1&0\\0&0&1\\0&0&0\end{bmatrix}\begin{bmatrix}x_1\\x_2\\x_3\end{bmatrix}+\begin{bmatrix}b_0\\0\\0\end{bmatrix}u+\begin{bmatrix}0\\0\\1\end{bmatrix}h \tag{6}$$

where $x_1=V_{DC}^2$, $x_2=f_{total}=-\frac{2}{C}(P_{ext}+\frac{V_{DC}^2}{R_p})$, $x_3=\dot{f}_{total}$, $u=P_s$, $b_0=\frac{2}{C}$, $h=\frac{dx_3}{dt}$

In order to enhance the estimation precision and also enable easier practical implementation, a new RGPIO is constructed for the DC-link voltage control. As shown in Fig.2, the control structure includes the outer loop and inner loop control strategy. In order to avoid the dynamic interaction between the outer loop DC-link voltage control and inner loop current control, the dynamic response of the current loop is usually assumed to be

much faster than that of voltage loop [41], which implies that the dynamic of the current loop can be neglected when designing the DC-link voltage control loop.

By re-writing (6), the following equations are derived as:

$$\begin{bmatrix}\dot{x}_2\\ \dot{x}_3\end{bmatrix}=\begin{bmatrix}0 & 1\\ 0 & 0\end{bmatrix}\begin{bmatrix}x_2\\ x_3\end{bmatrix}+\begin{bmatrix}0\\ 1\end{bmatrix}h \tag{7}$$

$$\dot{x}_1-b_0u=x_2 \tag{8}$$

Therefore, the RGPIO is designed as:

$$\begin{bmatrix}\dot{z}_2\\ \dot{z}_3\end{bmatrix}=\begin{bmatrix}0 & 1\\ 0 & 0\end{bmatrix}\begin{bmatrix}z_2\\ z_3\end{bmatrix}-\begin{bmatrix}k_1 & 0\\ k_2 & 0\end{bmatrix}\begin{bmatrix}z_2\\ z_3\end{bmatrix}+\begin{bmatrix}k_1\dot{x}_1\\ k_2\dot{x}_1\end{bmatrix}-\begin{bmatrix}k_1b_0u\\ k_2b_0u\end{bmatrix} \tag{9}$$

where $\begin{bmatrix}k_1\\ k_2\end{bmatrix}$ are the reduced-order GPIO gain, z_2 and z_3 are the estimated value of x_2 and x_3.. In Eq.(9), the variable $\dot{x}_1$ cannot be directly measured, hence, by manipulating $\begin{bmatrix}k_1\dot{x}_1\\ k_2\dot{x}_1\end{bmatrix}$ into the left hand of the equation, meanwhile, by adding and subtracting the term $\begin{bmatrix}-k_1 & 1\\ -k_2 & 0\end{bmatrix}\begin{bmatrix}k_1x_1\\ k_2x_2\end{bmatrix}$, the following observer equations are derived as:

$$\begin{bmatrix}\dot{z}_2\\ \dot{z}_3\end{bmatrix}-\begin{bmatrix}k_1\dot{x}_1\\ k_2\dot{x}_1\end{bmatrix}=\begin{bmatrix}-k_1 & 1\\ -k_2 & 0\end{bmatrix}\left\{\begin{bmatrix}z_2\\ z_3\end{bmatrix}-\begin{bmatrix}k_1x_1\\ k_2x_1\end{bmatrix}\right\}-\begin{bmatrix}k_1b_0u\\ k_2b_0u\end{bmatrix}+\begin{bmatrix}-k_1 & 1\\ -k_2 & 0\end{bmatrix}\begin{bmatrix}k_1x_1\\ k_2x_1\end{bmatrix} \tag{10}$$

It is observed from (10) that signals f_{total} and $\dot{f}_{total}$ can be observed by the proposed RGPIO. However, $\dot{f}_{total}$ can not be estimated by the ESO. It is true that RGPIO can estimate the derivative of the lumped disturbances, while the ESO based observer cannot achieve it. Meanwhile, the order of the presented RGPIO is only two. This reduced-order feature can reduce the computation burden to some extent.

B. System Stability Analysis

By subtracting (7) from (9), the error model of the proposed observer is obtained for stability analysis, the error equation is written as:

$$\begin{bmatrix}\dot{e}_1\\ \dot{e}_2\end{bmatrix}=\underbrace{\begin{bmatrix}-k_1 & 1\\ -k_2 & 0\end{bmatrix}}_{A_e}\begin{bmatrix}e_1\\ e_2\end{bmatrix}+\begin{bmatrix}k_1\dot{x}_1\\ k_2\dot{x}_1\end{bmatrix}-\begin{bmatrix}b_0u\\ b_0u\end{bmatrix} \tag{11}$$

From (11), it is observed that the system will be Hurwitz stable if both of the roots of the characteristic polynomial in the matrix A_e,i.e

$$\lambda(\mathrm{s})=\mathrm{s}^2+k_1s+k_2 \tag{12}$$

are in the left half-plane, in order to simplify the design process, it is assumed the poles of the observer are both located at $-\omega_0$, and are expressed as:

$$\lambda(\mathrm{s})=\mathrm{s}^2+k_1s+k_2=(s+\omega_0)^2 \tag{13}$$

Therefore, $\beta_1=2\omega_0$, $\beta_2=\omega_0^2$. From (13) it is shown that the design of the parameter k_1 and k_2 is related to the bandwidth (ω_0) of RGPIO. Therefore, the key process is to select the appropriate bandwidth ω_0. According to [42], the observer's bandwidth is normally selected to be 5-15 times larger than the DC link voltage controller's bandwidth by considering the trade-off between the fast observation performance and noise sensitivity immunity. The DC-link voltage controller's bandwidth is selected to be 20 rad/s, and the bandwidth of RGPIO is selected as 300 rad/s.

C. Frequency Domain Analysis for the RGPIO

By substituting $z_2-k_1x_1=\xi_2$ and $z_3-k_2x_1=\xi_3$, (10) is expressed as:

$$\begin{bmatrix}\dot{\xi}_2\\ \dot{\xi}_3\end{bmatrix}=\begin{bmatrix}-k_1 & 1\\ -k_2 & 0\end{bmatrix}\begin{bmatrix}\xi_2\\ \xi_3\end{bmatrix}+\begin{bmatrix}-k_1b_0 & -k_1^2+k_2\\ -k_2b_0 & -k_1k_2\end{bmatrix}\begin{bmatrix}u\\ x_1\end{bmatrix} \tag{14}$$

After replacing $k_1=2\omega_0$, $k_2=\omega_0^2$ into (14), the RGPIO is constructed as:

$$\begin{bmatrix}\dot{\xi}_2\\ \dot{\xi}_3\end{bmatrix}=\underbrace{\begin{bmatrix}-2\omega_0 & 1\\ -\omega_0^2 & 0\end{bmatrix}}_{A_z}\begin{bmatrix}\xi_2\\ \xi_3\end{bmatrix}+\begin{bmatrix}-2\omega_0b_0 & -3\omega_0^2\\ -\omega_0^2b_0 & -2\omega_0^3\end{bmatrix}\begin{bmatrix}u\\ x_1\end{bmatrix} \tag{15}$$

Eq.(15) can be converted into transfer functions by taking the following equation:

$$G_{\xi_2\_u}(s)=\frac{\xi_2(s)}{u(s)}=-\frac{b_0\omega_0^2}{(s+\omega_0)^2}-\frac{2b_0\omega_0 s}{(s+\omega_0)^2} \tag{16}$$

$$G_{\xi_2 V_{DC}^2}(s)=\frac{\xi_2(s)}{V_{DC}^2(s)}=-\frac{2\omega_0^3}{(s+\omega_0)^2}-\frac{3\omega_0^2 s}{(s+\omega_0)^2} \tag{17}$$

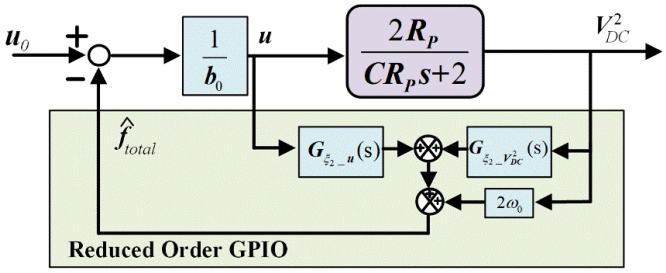

Fig.3. The equivalent transfer function of RGPIO in the DC-link voltage control

As $z_2-k_1x_1=\xi_2$, and $x_1=V_{DC}^2$, $k_1=2\omega_0$. Therefore, by combing (11) and (12) and substitute $z_2-k_1x_1=\xi_2$, the transfer function of reduced-order GPIO is shown in Fig.3. The modified model from u_0 to $V_{DC}^2(s)$ can be expressed as the transfer function $\overline{\mathrm{G}_p}(s)$:

$$\overline{\mathrm{G}_p}(s)=\frac{V_{DC}^2(s)}{u_o\,(s)}=\frac{\dfrac{G_p}{b_0}}{1-\dfrac{1}{\left(\frac{s}{\omega_0}+1\right)^2}-\dfrac{2\left(\frac{s}{\omega_0}\right)}{\left(\frac{s}{\omega_0}+1\right)^2}+\left(\dfrac{G_p}{b_0}\right)\dfrac{\left(s+\frac{2s}{\omega_0^2}\right)}{\left(\frac{s}{\omega_0}+1\right)^2}} \tag{18}$$

It is found from Eq.(18) that within the RGPIO's bandwidth ω_0, the system transfer function is simplified to be an integrator and shown as:

$$\overline{\mathrm{G}_p}(s)\approx\frac{1}{s}\qquad\omega\ll\omega_0 \tag{19}$$

From (19), it is observed that by incorporating the RGPIO into the control strategy, the original plant is modified into an ideal integrator within the bandwidth of ω_0 . It is noted that the modified plant returns to the original plant beyond the bandwidth of ω_0.

D. Evaluation of the system robustness against parameter variation

The DC-link capacitance variation may have an influence on the system's dynamic performance and stability. Therefore, the system's closed-loop poles should be evaluated to examine the system's robustness against the capacitance parameter's variation. In the test, the nominal value of the DC-link capacitance is selected to be 1100μF, but due to the connection

of the battery or the UPS system in the DC link, the actual DC-link capacitance may have variation from its nominal value. Hence, the poles' location with the model $\overline{G_p}(s)$ is evaluated when the actual capacitance changes from 1100μF to 3300μF. It is observed from Fig.4 that when the DC-link capacitance increases, the closed-loop poles tend to move to the imaginary axis, which makes the system more unstable. However, even the capacitance has changed to 3300μF, the dominant pole still has distance from the imaginary axis, which means the system can provide satisfactory robustness.

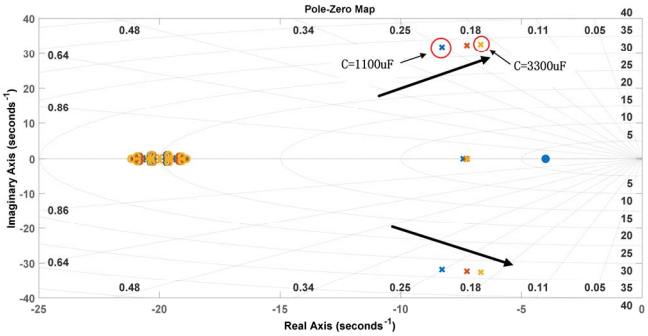

Fig.4. Pole's movement when the DC-link capacitance value change from 1100μF to 3300μF.

E. DC-link Voltage Controller

As is shown in the previous section, when the RGPIO is embedded in the DC-link voltage control, the plant has been changed to be an integrator ($\overline{G_p}(s) \approx \frac{1}{s}$), which means a proportional controller can regulate the DC-link voltage without steady-state error. Therefore, by considering the approximated transfer function of the modified plant, the closed-loop transfer function of the DC-link voltage loop is expressed as:

$$G_{v\_c} \approx \frac{k_p \frac{1}{s}}{1+k_p \frac{1}{s}} = \frac{k_p}{k_p+s} = \frac{1}{1+s/k_p} \tag{20}$$

From the above discussion, it is shown that the proposed RGPIO is responsible for canceling the lumped disturbance, and then a simple proportional controller is able to track the voltage reference without steady-state error.

IV. The Inner Loop RST-SMC Based Current Tracking Design

The goal of the inner control loop is to make sure that the inductor's sinusoidal currents in the stationary frame i_α and i_β track the reference currents i_α^* and i_β^*. The reference current is expressed as [30] :

$$i_\alpha^* = \frac{2}{3}\frac{V_{g\alpha}}{V_{g\alpha}^2+V_{g\beta}^2}P_{s\_ref} + \frac{2}{3}\frac{V_{g\beta}}{V_{g\alpha}^2+V_{g\beta}^2}Q_{s\_ref} \tag{21}$$

$$i_\beta^* = \frac{2}{3}\frac{V_{g\beta}}{V_{g\alpha}^2+V_{g\beta}^2}P_{s\_ref} - \frac{2}{3}\frac{V_{g\alpha}}{V_{g\alpha}^2+V_{g\beta}^2}Q_{s\_ref} \tag{22}$$

It is noted that the active power reference (P_{s_ref}) is generated from the output of the DC-link voltage controller (see Fig.2), and the reactive power reference (Q_{s_ref}) is set to the desired value.

A. Super-Twisting Control

In order to achieve fast current tracking, the traditional SMC is usually applied as the inner loop controller. However, the main drawback of the traditional SMC is the chattering issue, which leads to the discontinuous high switching frequency. To overcome this issue, the ST-SMC has been proposed in [43]. ST-SMC is a second-order controller and the state's trajectory in the state plane shifts in a spiral pattern and converges to the original state asymptotically in finite time. In general, consider a nonlinear controlled system

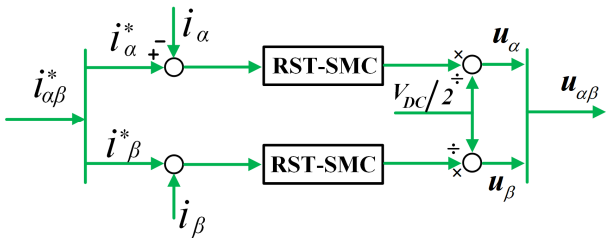

Fig.5. Block diagram of the details of proposed RST-SMC.

$$\dot{x} = a(x) + b(x)u \tag{23}$$

$$y = \sigma(t,x) \tag{24}$$

where $x \in \mathcal{R}^n$ is the stage vector, $u \in \mathcal{R}$ represent the control input, $\sigma(t,\ x)$ is the sliding variable, $a(x)$ and $b(x)$ are the smooth uncertain functions.

In the ST-SMC, the control goal is to force σ and its derivative $\dot{\sigma}$ to zero. Hence, by differentiating the sliding variable $\sigma(t,x)$ twice, the following expression can be derived as :

$$\ddot{\sigma} = h(t,x,u) + g(t,x,u)\dot{u} \tag{25}$$

where $h(t,x,u)$ and $g(t,x,u)$ are bounded but unknown, there exist positive constant values Φ, Γ_m, Γ_M, such that the following conditions are satfisied:

$$0 < \Gamma_m < g(t,x,u) < \Gamma_M \tag{26}$$

$$-\Phi \le h(t,x,u) \le \Phi \tag{27}$$

Then, a differential inclusion can be expressed as:

$$\ddot{\sigma} \in [-\Phi \quad +\Phi] + [\Gamma_m \quad \Gamma_M]\dot{u} \tag{28}$$

With the condition of (26) and (27), a differential inclusion is obtained:

$$\ddot{s} \in [-\Phi, \quad \Phi] + [\Gamma_m, \quad \Gamma_M]\dot{u} \tag{29}$$

Thus, a control law based on a super-twisting algorithm (STA) can be designed as:

$$\begin{cases} u = -\lambda|\sigma|^{\frac{1}{2}}\text{sign}(\sigma) + v \\ \dot{v} = -\mu\text{sgn}(\sigma) \end{cases} \tag{30}$$

Where λ and μ are the design parameters that can be determined by the boundary conditions (26) and (27). In addition, the parameters can be chosen as following to make sure the sliding variable σ can be converged to the sliding manifold in finite time:

$$\mu > \frac{\Phi}{\Gamma_m}, \lambda^2 > \frac{4\Phi}{\Gamma_m^2}\frac{\Gamma_M}{\Gamma_m}\frac{\mu+\Phi}{\mu-\Phi} \tag{31}$$

B. Current tracking loop

In the current tracking loop, two procedures are needed to design the ST-SMC. First, we need to choose a proper sliding surface where the system states are driven to zero. The second step is to design the control law, which brings the system states on the sliding surface and always keeps them stay in the sliding surface.

First, the sliding surface equations for the current control are defined as:

$$\sigma_\alpha = i_\alpha^* - i_\alpha \tag{32}$$

$$\sigma_\beta = i_\beta^* - i_\beta \tag{33}$$

In addition, in order to reject grid voltage disturbance and achieve zero steady-state reference tracking, the resonant term $\frac{Cs}{s^2+(\omega)^2}$ is added in (37), the final designed RST-SMC strategy are shown in (38) and (39) in Laplace domain:

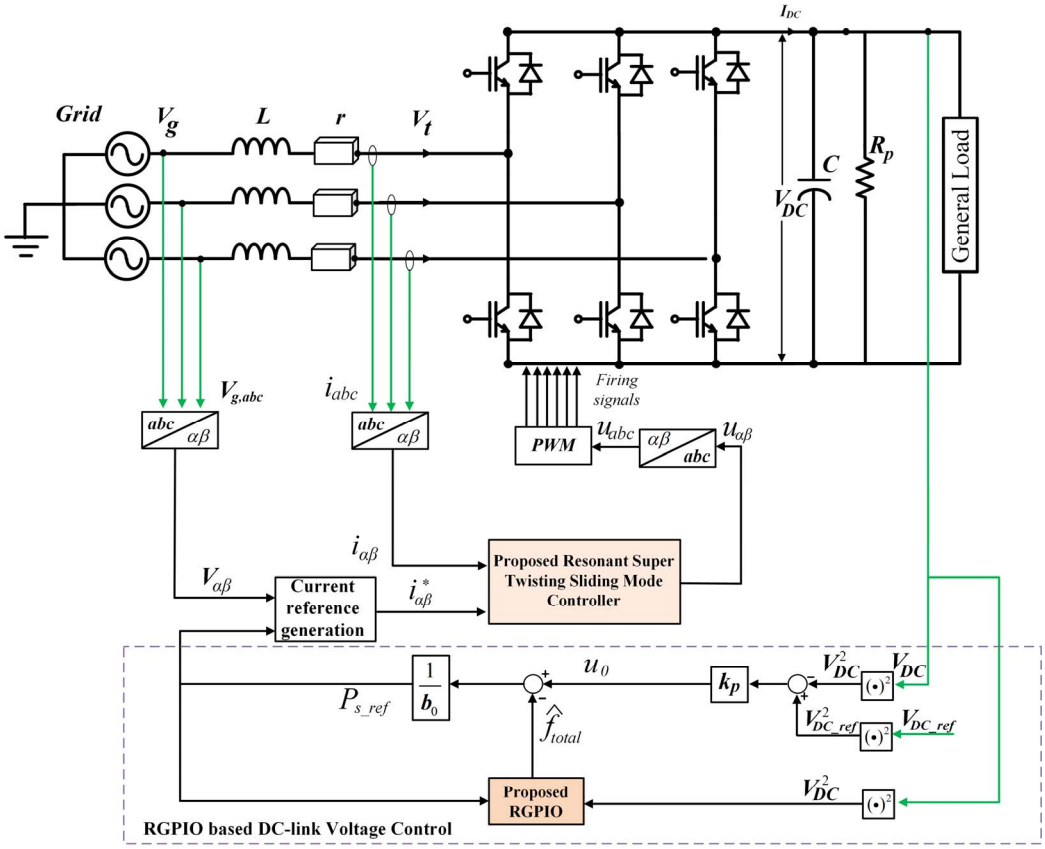

Fig.6. Schematic diagram of the RGPIO based RST-SMC strategy for the three-phase AC/DC converter.

The control law is derived by introducing a candidate Lyapunov function as [43] :

$$\mathrm{W} = \frac{1}{2}\sigma_{\alpha\beta}^T\sigma_{\alpha\beta} > 0 \tag{34}$$

where $\sigma_{\alpha\beta} = [\sigma_\alpha\ \sigma_\beta]^T$. The time derivative of the above Lyapunov function is calculated as:

$$\frac{d\mathrm{W}}{dt} = \frac{1}{2}\left(\sigma_{\alpha\beta}^T\frac{d\sigma_{\alpha\beta}}{dt} + \sigma_{\alpha\beta}\frac{d\sigma_{\alpha\beta}^T}{dt}\right) = \sigma_{\alpha\beta}^T\frac{d\sigma_{\alpha\beta}}{dt} \tag{35}$$

According to Eq.(1), (32) and (33), the time derivative of $\sigma_{\alpha\beta}$ is expressed as:

$$\frac{d\sigma_{\alpha\beta}}{dt} = \frac{d}{dt}\begin{bmatrix}\sigma_\alpha\\ \sigma_\beta\end{bmatrix} = \begin{bmatrix}i_\alpha^* + \frac{r}{L}i_\alpha\\ i_\beta^* + \frac{r}{L}i_\beta\end{bmatrix} - \frac{1}{L}\begin{bmatrix}V_{g\alpha}\\ V_{g\beta}\end{bmatrix} + \frac{1}{L}\begin{bmatrix}V_{t\alpha}\\ V_{t\beta}\end{bmatrix} \tag{36}$$

Therefore, as long as choosing an appropriate positive value of A and B in Eq.(37), the following ST-SMC in Eq.(37) makes sure $\frac{d\mathrm{W}}{dt} < 0$. Hence, the system stability is guaranteed

$$\begin{bmatrix}V_{t\alpha}\\ V_{t\beta}\end{bmatrix} = \begin{bmatrix}-A|\sigma_\alpha|^{\frac{1}{2}}\mathrm{sgn}(\sigma_\alpha) - B\int_0^t \mathrm{sgn}(\sigma_\alpha)d\tau\\ -A|\sigma_\beta|^{\frac{1}{2}}\mathrm{sgn}(\sigma_\beta) - B\int_0^t \mathrm{sgn}(\sigma_\beta)d\tau\end{bmatrix} \tag{37}$$

$$V_{t\alpha}(s) = -\left[A|\sigma_\alpha|^{\frac{1}{2}}\mathrm{sgn}(\sigma_\alpha) + B\mathrm{sgn}(\sigma_\alpha)\cdot\frac{1}{s} + (\frac{Cs}{s^2+(\omega)^2})\sigma_\alpha\right] \tag{38}$$

$$V_{t\beta}(s) = -\left[A|\sigma_\beta|^{\frac{1}{2}}\mathrm{sgn}(\sigma_\beta) + B\mathrm{sgn}(\sigma_\beta)\cdot\frac{1}{s} + (\frac{Cs}{s^2+(\omega)^2})\sigma_\beta\right] \tag{39}$$

where parameters A and B are selected according to Eq.(28)-(30). In addition, by assuming the $\Gamma_m = \Gamma_M$, the parameters for A and B are selected as: $A^2 \geq 4M\frac{B+M}{B-M}$, $B > M$, M is upper bound of the grid voltage amplitude. Parameter C is designed based on the resonant controller's design principle, a simple method to determine the parameter C is angular frequency squared times inductance [44].

Therefore, (38) and (39) indicate the dynamic behavior of the RST-SMC, the system disturbance is rejected by the resonant term, and the output current is compelled to follow the reference ac current by ST-SMC in the sliding surface with maximum stability.

Fig.5 shows the block diagram of the proposed RST-SMC strategy. And the full control diagram, including the proposed RGPIO based control and RST-SMC strategy, is shown in

Fig.6. In the DC-link voltage regulation, an RGPIO based proportional controller is adopted to achieve both DC link voltage regulation and the load disturbance rejection; meanwhile, the inner loop RST-SMC strategy is implemented for the fast current regulation.

In practical application, the current controller's performance can be affected by the system parameter variation; therefore, (36) can be expressed as:

$$\frac{d\sigma_{\alpha\beta}}{dt}=\frac{d}{dt}\begin{bmatrix}\sigma_\alpha\\ \sigma_\beta\end{bmatrix}=\begin{bmatrix}i_\alpha^{*}+\frac{r}{L}i_\alpha\\ i_\beta^{*}+\frac{r}{L}i_\beta\end{bmatrix}-\frac{1}{L}\begin{bmatrix}V_{g\alpha}\\ V_{g\beta}\end{bmatrix}+\frac{1}{L}\begin{bmatrix}V_{t\alpha}\\ V_{t\beta}\end{bmatrix}+\frac{\Delta L}{L}\begin{bmatrix}\dot{i}_\alpha\\ \dot{i}_\beta\end{bmatrix} \quad (40)$$

where ΔL represents the inductance's parameter variation. In addition, considering that grid voltage disturbance is rejected and canceled by the resonant terms of the proposed controller, and if the positive control gains of A and B are set to be large enough, system stability can still be satisfied and expressed as

$$\frac{dW}{dt}=\sigma_{\alpha\beta}^{T}\frac{d\sigma_{\alpha\beta}}{dt}=-\frac{1}{L}\sigma_{\alpha\beta}\left(A\left|\sigma_{\alpha\beta}\right|^{\frac{1}{2}}\mathrm{sgn}\left(\sigma_{\alpha\beta}\right)+B\int_0^t\mathrm{sgn}\left(\sigma_{\alpha\beta}\right)d\tau-H\right)<0 \quad (41)$$

where $\sigma_{\alpha\beta}\cdot\mathrm{sgn}\left(\sigma_{\alpha\beta}\right)>0$, $H=[H_1 \quad H_2]^T$ and is expressed in Eq.(42):

$$\begin{bmatrix}H_1\\ H_2\end{bmatrix}=\begin{bmatrix}i_\alpha^{*}+\frac{r}{L}i_\alpha\\ i_\beta^{*}+\frac{r}{L}i_\beta\end{bmatrix}+\frac{\Delta L}{L}\begin{bmatrix}\dot{i}_\alpha\\ \dot{i}_\beta\end{bmatrix} \quad (42)$$

V. Simulation Results

This section provides simulation results obtained from the proposed control strategy and the standard control strategy. In this paper, the PI control strategy for the DC-link voltage regulation with a proportional resonant (PR) control strategy for the inner current regulation is adopted as the standard control strategy. The simulations are carried out in Matlab/Simulink with the AC/DC converter configuration shown in Fig.1. Table I shows the control parameters and the electric parameters of the converter.

A. Operation under load resistance variation

In this test, the sharp load resistance is changed from 1500Ω to 150 Ω to test the controller's dynamic performance, Fig.7 shows the simulation results for the proposed control strategy and the PI control strategy. It should be mentioned that both controllers are tuned to be the same bandwidth to have a fair comparison. It can be observed that although the PI control strategy can recover to the original voltage within 1s, it takes longer time than the proposed control strategy. The undershoot with the proposed control strategy is 30V. On the contrary, 60V of the undershoot is observed with the PI control strategy. Meanwhile, the transient current on the grid side presents a faster response with the proposed control strategy.

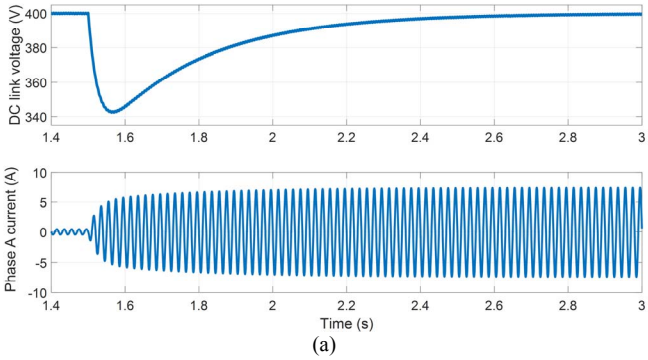

(a)

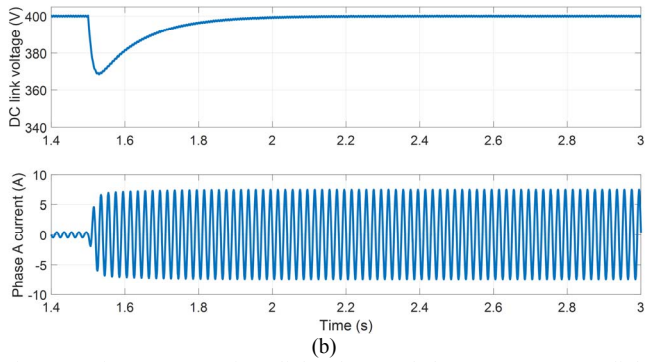

(b)

Fig.7.Transient response of DC-link voltage and phase current. (a) DC-link voltage and phase current with PI control strategy, (b) DC-link voltage and phase current with the proposed control strategy.

B. Operation with Current Command Step

The second simulation assesses the current control strategy capability to provide a desired amount of reactive power. The reactive power command step is introduced from 0 to 1.6kVar. The system's response is evaluated for both PR control strategy and the RST-SMC strategy. It can be found from Fig.8 (a) that when the reactive power step changes, the current in α frame has an overshoot of 3A. On the contrary, Fig.8 (b) shows the current response when the same amount of the reactive power step changes, it is observed that the current almost does not cause overshoot with the proposed control strategy.

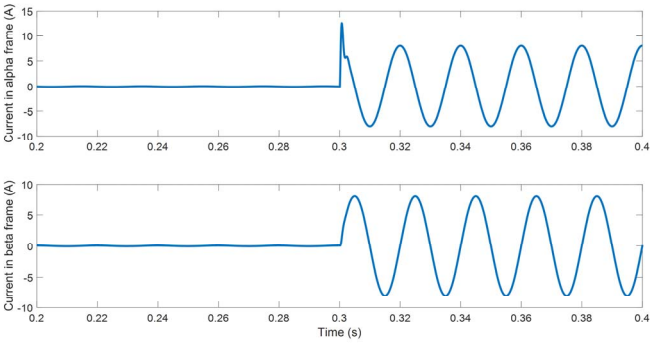

(a)

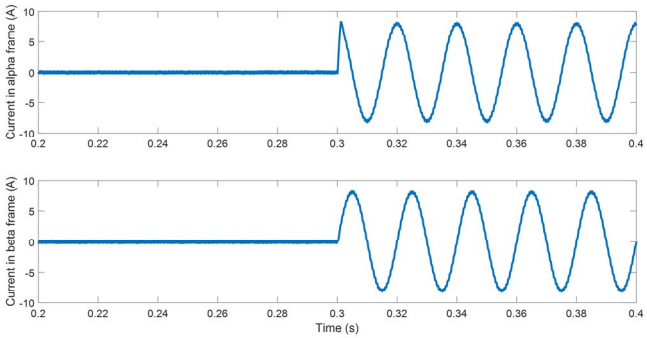

(b)

Fig.8. Transient response of the grid current in $\alpha - \beta$ frame with the reactive power step change (a) grid current with standard PR control strategy, (b) grid current with the proposed control strategy

VI. EXPERIMENTAL RESULTS

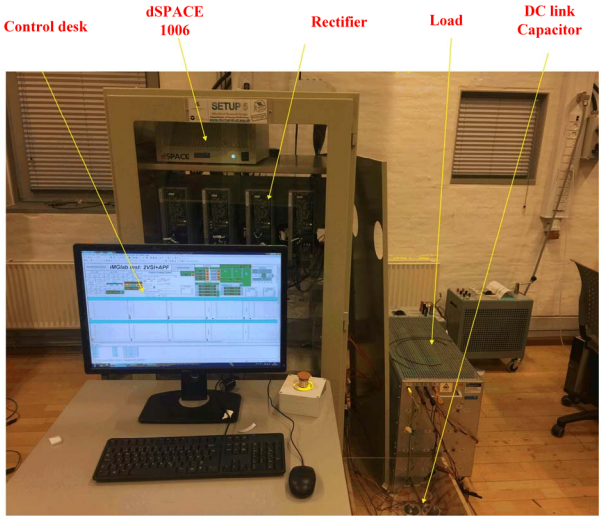

Fig.9. Experimental setup

In order to verify the effectiveness of the proposed control strategy, an AC/DC converter illustrated in Fig.1 is built up in Fig.9, The system parameter is shown in Table I. The sampling frequency is chosen to be 10kHz, the comparative experimental results are provided from the standard control strategy (outer loop PI control with inner loop PR control strategy) and the proposed control strategy, these control strategies are both controlled by dSPACE 1006 controller for comparison. The experimental results are shown in Fig.10-Fig.13 for both standard method and the proposed control strategy.

TABLE I. SYSTEM PARAMETER

AC/dc Inverter Parameters	
Filter inductor L	1.8mH
Inductor's parasitic resistance	0.04Ω
Sampling frequency f_s	10kHz
DC link voltage	400V
Grid RMS Voltage	120V
DC-link capacitance	1100μF
Control Parameters in RST-SMC	
Parameter A	35
Parameter B	10000
Parameter C	500
PR Controller Parameters for comparison	
Proportional gain	35
Resonant Controller	1000
RGPIO Controller Parameter	
Proportional gain	20
DC-link voltage controller with PI controller for comparison	
Proportional gain	0.2
Integral gain	1

A. Dynamic performance under load step change

The dynamic performance of the standard PI control strategy and the proposed control strategy with the load disturbance are exhibited in Fig.10, where the external load is suddenly changed from light load (1500 Ω) to full load (150 Ω). For the DC-link voltage loop control, the voltage loop is usually chosen to be 0.05-0.2 times the bandwidth of the current loop in order to avoid the interaction of the voltage loop and the current loop and avoid the stability issue. And the current loop is usually chosen to be 0.1 times the bandwidth of the sampling frequency. Therefore, the voltage loop usually is chosen to be 0.005-0.02 times the bandwidth of the sampling frequency. It should be noted that a very fast DC-link voltage is not necessary, as the DC-link capacitor is usually large, and consequently, the DC-bus voltage cannot rapidly be changed. In order to have a fair comparison, the bandwidth of both DC-link voltage controllers are the same, and it can be observed that both control laws can achieve the DC-link voltage regulation. However, their dynamic performances are quite different. To be more specific, it is shown that with the PI control strategy, the DC link voltage has an undershoot of 60V, and it takes around 1s to track the reference voltage after the load variation. On the contrary, as the disturbance caused by the load variation is actively canceled by the RGPIO, the DC link voltage dips around only 30V, and the recovery time is around 0.4s with the proposed control strategy. Fig.10 (c) and (d) show the phase A output current with the load variation. It is demonstrated that current with the proposed control strategy has a faster speed than the PI control strategy. In addition, it should be mentioned that the PI control strategy in the experiment works in the

operating point, which does not cause the wind-up phenomenon in the system. If the overloading occurs in the system, due to the proportional controller, the proposed control strategy does not lead to the wind-up phenomenon; On the contrary, the PI control strategy has to add the anti-windup algorithm to prevent the windup [44, 45].

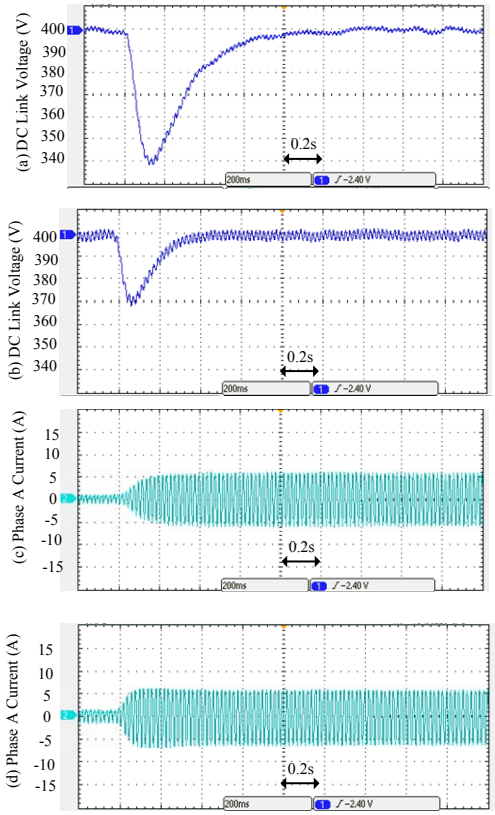

Fig. 10. Experimental results of the load variation （a) DC-link voltage with PI control (b) DC-link voltage with proposed control strategy (c) phase A current with PI control (d) phase A current with the proposed control strategy

B. Dynamic performance under DC-link voltage increase

The dynamic performance of the standard and the proposed control strategies are compared with the DC-link voltage demand variations. The comparison results are shown in Fig.11. It can be obviously seen that both methods can regulate the DC-link voltage to the settling point. The DC link voltage steps up from 400V to 420V, and it takes 0.6s for the PI control strategy to reach a new steady-state. On the contrary, it only takes 0.3s to reach the same steady-state operating point, where the response time is reduced by 50%. It is noted that the proposed controller could achieve a faster dynamic response, which causes the active power reference overshoot to be larger than that of the PI control strategy, but the settling time of active power reference in the proposed control strategy is shorter than that in the PI control strategy.

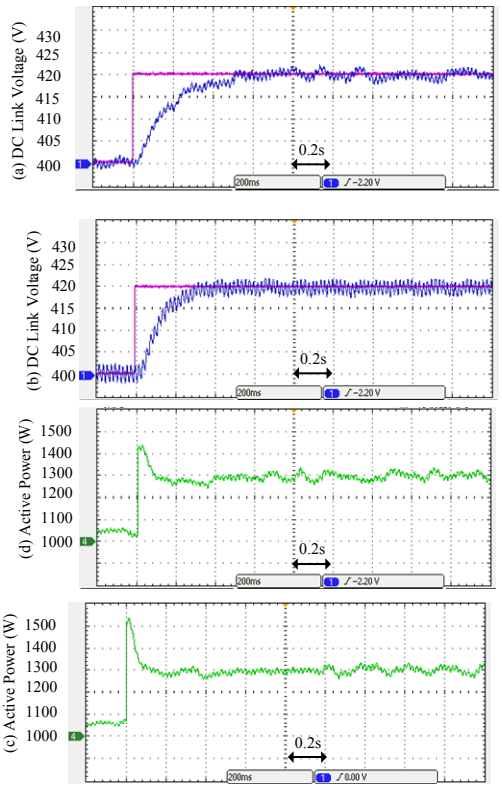

Fig. 11. Experimental results for the DC-link voltage reference increase (a) DC-link voltage with PI control, (b) DC-link voltage with the proposed control strategy. (c) Active power with PI control (d) Active power with the proposed control strategy

C. Current loop performance with current reference step change

In order to verify the proposed current control strategy, the comparison between the PR control strategy and the proposed control strategy is tested. In order to observe the difference between these two control strategies, the current is transformed from the $\alpha - \beta$ frame to the d-q frame. When the reference current in q-axis has a step change from 0A to 8A, it is observed in Fig.12 (a), in the PR control strategy, the q-axis current has an overshoot of 2A and the settling time is 5ms; meanwhile, this step change leads to the overshoot current of 1.7A in the d-axis. In contrast, the proposed control approach has an overshoot of 1A with the settling time of dfda2ms (see Fig.12(b)). At the same time, the coupling influence of the proposed control strategy is almost the same as the PR control strategy. It is noted that if the excessive loading occurs, it may cause the output of the current controller to saturate. There are several ways to prevent the windup; one straightforward method is known as back calculation [46].

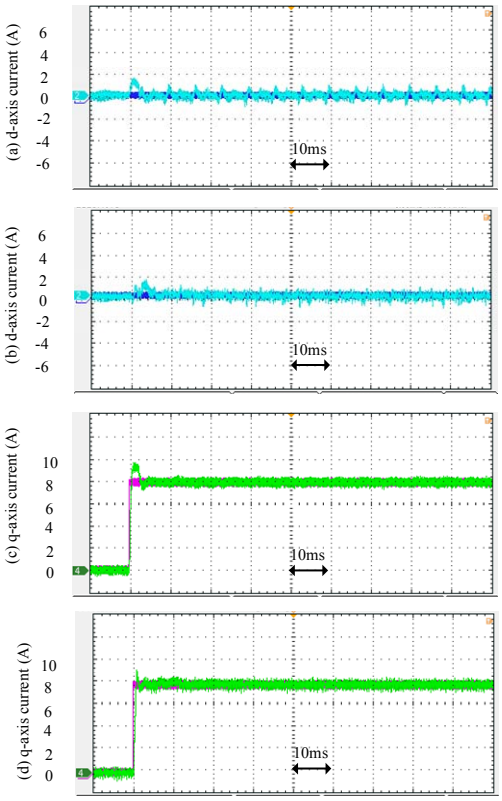

Fig. 12. Experimental results for the transient response with reactive power step-up (a) d-axis current with the standard control strategy, (b) d-axis current with the proposed control strategy. (c) q-axis current with the standard control strategy (d) q-axis current with the proposed control strategy

D. THD of the current at the steady-state

Fig.13 shows the comparison of the steady-state current with the reactive power command. It is observed that the proposed current control strategy has better performance, especially the 5th and 7th harmonics are reduced compared with the PR control strategy. Furthermore, the current THD for the RGPIO-RST-SMC strategy is 1.3% and 1.6% for the standard one.

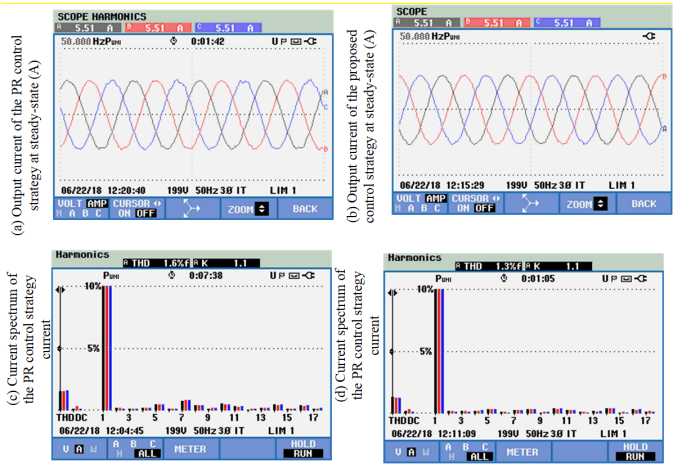

Fig.13. Experimental results of the steady-state current with reactive power command (a) current waveform for the PR control strategy; (b) current waveform for the proposed control strategy; (c) spectrum of the current with PR control strategy; (d) spectrum of the current with the proposed control strategy

VII. CONCLUSION

In this paper, an RGPIO based RST-SMC strategy was proposed for the three-phase AC/DC converter. By applying the proposed RGPIO based control strategy for DC-link voltage regulation, the system's dynamic response under the disturbance was greatly improved, and the settling time was reduced compared with the traditional one. The proposed RST-SMC current control strategy was proposed for the reference tracking in $\alpha-\beta$ frame under the system parameter uncertainty. Experimental results showed the effectiveness of the proposed control strategy and demonstrated better performance compared with the standard control strategy.

Reference

[1] J. M. Carrasco *et al.*, "Power-Electronic Systems for the Grid Integration of Renewable Energy Sources: A Survey," *Ieee T Ind Electron,* vol. 53, no. 4, pp. 1002-1016, 2006, doi: 10.1109/TIE.2006.878356.

[2] C. Zhang, J. M. Guerrero, J. C. Vasquez, and E. A. A. Coelho, "Control Architecture for Parallel-Connected Inverters in Uninterruptible Power Systems," *Ieee T Power Electr,* vol. 31, no. 7, pp. 5176-5188, 2016, doi: 10.1109/TPEL.2015.2481480.

[3] Q. Xu *et al.*, "Analysis and Comparison of Modular Railway Power Conditioner for High-Speed Railway Traction System," *Ieee T Power Electr,* vol. 32, no. 8, pp. 6031-6048, 2017, doi: 10.1109/TPEL.2016.2616721.

[4] P. C. Loh, D. Li, Y. K. Chai, and F. Blaabjerg, "Hybrid AC&DC Microgrids With Energy Storages and Progressive Energy Flow Tuning," *Ieee T Power Electr,* vol. 28, no. 4, pp. 1533-1543, 2013, doi: 10.1109/TPEL.2012.2210445.

[5] J. Lu *et al.*, "DC-Link Protection and Control in Modular Uninterruptible Power Supply," *Ieee T Ind Electron,* vol. PP, no. 99, pp. 1-1, 2017, doi: 10.1109/TIE.2017.2760847.

[6] J. Dannehl, C. Wessels, and F. W. Fuchs, "Limitations of Voltage-Oriented PI Current Control of Grid-Connected PWM Rectifiers With LCL Filters," *Ieee T Ind Electron,* vol. 56, no. 2, pp. 380-388, 2009, doi: 10.1109/TIE.2008.2008774.

[7] D. N. Zmood and D. G. Holmes, "Stationary frame current regulation of PWM inverters with zero steady-state error," *Power Electronics, IEEE Transactions on,* vol. 18, no. 3, pp. 814-822, 2003, doi: 10.1109/TPEL.2003.810852.

[8] L. Harnefors, A. G. Yepes, A. Vidal, and J. Doval-Gandoy, "Passivity-Based Controller Design of Grid-Connected VSCs for Prevention of Electrical Resonance Instability," *Industrial Electronics, IEEE Transactions on,* vol. 62, no. 2, pp. 702-710, 2015, doi: 10.1109/TIE.2014.2336632.

[9] S. Vazquez *et al.*, "Model Predictive Control: A Review of Its Applications in Power Electronics," *IEEE Industrial Electronics Magazine,* vol. 8, no. 1, pp. 16-31, 2014, doi: 10.1109/MIE.2013.2290138.

[10] J. F. Silva, "Sliding-mode control of boost-type unity-power-factor PWM rectifiers," *Ieee T Ind Electron,* vol. 46, no. 3, pp. 594-603, 1999, doi: 10.1109/41.767067.

[11] S. C. Tan, Y. M. Lai, C. K. Tse, L. Martinez-Salamero, and C. K. Wu, "A Fast-Response Sliding-Mode Controller for Boost-Type Converters With a Wide Range of Operating Conditions," *Ieee T Ind Electron,* vol. 54, no. 6, pp. 3276-3286, 2007, doi: 10.1109/TIE.2007.905969.

[12] J. Liu, S. Vazquez, L. Wu, A. Marquez, H. Gao, and L. G. Franquelo, "Extended State Observer-Based Sliding-Mode Control for Three-Phase Power Converters," *Ieee T Ind Electron,* vol. 64, no. 1, pp. 22-31, 2017, doi: 10.1109/TIE.2016.2610400.

[13] H. Wang, X. Ge, and Y. C. Liu, "Second-Order Sliding-Mode MRAS Observer Based Sensorless Vector Control of Linear Induction Motor Drives for Medium-Low Speed Maglev Applications," *Ieee T Ind Electron,* pp. 1-1, 2018, doi: 10.1109/TIE.2018.2818664.

[14] R. Sadeghi, S. M. Madani, M. Ataei, M. R. A. Kashkooli, and S. Ademi, "Super-Twisting Sliding Mode Direct Power Control of

Brushless Doubly Fed Induction Generator," *Ieee T Ind Electron,* pp. 1-1, 2018, doi: 10.1109/TIE.2018.2818672.

[15] O. Kukrer, H. Komurcugil, and A. Doganalp, "A Three-Level Hysteresis Function Approach to the Sliding-Mode Control of Single-Phase UPS Inverters," *Ieee T Ind Electron,* vol. 56, no. 9, pp. 3477-3486, 2009, doi: 10.1109/TIE.2009.2016512.

[16] M. B. Delghavi and A. Yazdani, "Sliding-Mode Control of AC Voltages and Currents of Dispatchable Distributed Energy Resources in Master-Slave-Organized Inverter-Based Microgrids," *IEEE Transactions on Smart Grid,* vol. PP, no. 99, pp. 1-1, 2017, doi: 10.1109/TSG.2017.2756935.

[17] X. Zheng, Y. Feng, F. Han, and X. Yu, "Integral-Type Terminal Sliding-Mode Control for Grid-Side Converter in Wind Energy Conversion Systems," *Ieee T Ind Electron,* vol. 66, no. 5, pp. 3702-3711, 2019, doi: 10.1109/tie.2018.2851959.

[18] H. Li, W. Wu, M. Huang, H. Chung, M. Liserre, and F. Blaabjerg, "Design of PWM-SMC Controller Using Linearized Model for Grid-Connected Inverter with LCL Filter," *Ieee T Power Electr,* pp. 1-1, 2020, doi: 10.1109/tpel.2020.2990496.

[19] R. Guzman, L. G. d. Vicuña, M. Castilla, J. Miret, and H. Martín, "Variable Structure Control in Natural Frame for Three-Phase Grid-Connected Inverters With LCL Filter," *Ieee T Power Electr,* vol. 33, no. 5, pp. 4512-4522, 2018.

[20] T. He, D. D. Lu, L. Li, J. Zhang, L. Zheng, and J. Zhu, "Model-Predictive Sliding-Mode Control for Three-Phase AC/DC Converters," *Ieee T Power Electr,* vol. 33, no. 10, pp. 8982-8993, 2018.

[21] A. Levant, "Higher order sliding modes and arbitrary-order exact robust differentiation," in *2001 European Control Conference (ECC)*, 4-7 Sept. 2001 2001, pp. 996-1001, doi: 10.23919/ECC.2001.7076043.

[22] H. Xiang, Y. Xu, L. Tao, H. Lang, and C. Wenjie, "A Sliding-Mode Controller With Multiresonant Sliding Surface for Single-Phase Grid-Connected VSI With an LCL Filter," *Power Electronics, IEEE Transactions on,* vol. 28, no. 5, pp. 2259-2268, 2013, doi: 10.1109/TPEL.2012.2218133.

[23] A. Chalanga, S. Kamal, L. M. Fridman, B. Bandyopadhyay, and J. A. Moreno, "Implementation of Super-Twisting Control: Super-Twisting and Higher Order Sliding-Mode Observer-Based Approaches," *Ieee T Ind Electron,* vol. 63, no. 6, pp. 3677-3685, 2016, doi: 10.1109/TIE.2016.2523913.

[24] T. Gonzalez, J. A. Moreno, and L. Fridman, "Variable Gain Super-Twisting Sliding Mode Control," *IEEE Transactions on Automatic Control,* vol. 57, no. 8, pp. 2100-2105, 2012, doi: 10.1109/TAC.2011.2179878.

[25] X. Shen *et al.*, "High-Performance Second Order Sliding Mode Control for NPC Converters," *Ieee T Ind Inform,* pp. 1-1, 2019, doi: 10.1109/TII.2019.2960550.

[26] W. Luo, T. Zhao, X. Li, Z. Wang, and L. Wu, "Adaptive super-twisting sliding mode control of three-phase power rectifiers in active front end applications," *IET Control Theory & Applications,* vol. 13, no. 10, pp. 1483-1490, 2019, doi: 10.1049/iet-cta.2018.6141.

[27] R. Sadeghi, S. M. Madani, M. Ataei, M. R. A. Kashkooli, and S. Ademi, "Super-Twisting Sliding Mode Direct Power Control of a Brushless Doubly Fed Induction Generator," *Ieee T Ind Electron,* vol. 65, no. 11, pp. 9147-9156, 2018, doi: 10.1109/TIE.2018.2818672.

[28] Y. Yin *et al.*, "Adaptive Control for Three-Phase Power Converters With Disturbance Rejection Performance," *IEEE Transactions on Systems, Man, and Cybernetics: Systems,* pp. 1-12, 2019, doi: 10.1109/tsmc.2018.2876322.

[29] X. Shen *et al.*, "High-Performance Second-Order Sliding Mode Control for NPC Converters," *Ieee T Ind Inform,* vol. 16, no. 8, pp. 5345-5356, 2020.

[30] R. I. Amirnaser Yazdani, "Voltage-Sourced Converters in Power Systems : Modeling, Control, and Applications," 2010.

[31] C. Wang, X. Li, L. Guo, and Y. W. Li, "A Nonlinear-Disturbance-Observer-Based DC-Bus Voltage Control for a Hybrid AC/DC Microgrid," *Ieee T Power Electr,* vol. 29, no. 11, pp. 6162-6177, 2014, doi: 10.1109/TPEL.2013.2297376.

[32] J. Liu, X. Tao, M. Yu, Y. Xia, and W. Wei, "Impedance Modeling and Analysis of Three-Phase Voltage-Source Converters Viewing From DC Side," *IEEE Journal of Emerging and Selected Topics in Power Electronics,* pp. 1-1, 2019, doi: 10.1109/JESTPE.2019.2932618.

[33] Y. Yin *et al.*, "Adaptive Control for Three-Phase Power Converters With Disturbance Rejection Performance," *IEEE Transactions on Systems, Man, and Cybernetics: Systems,* pp. 1-12, 2018, doi: 10.1109/TSMC.2018.2876322.

[34] M. Davari and Y. A. R. I. Mohamed, "Robust Multi-Objective Control of VSC-Based DC-Voltage Power Port in Hybrid AC/DC Multi-Terminal Micro-Grids," *IEEE Transactions on Smart Grid,* vol. 4, no. 3, pp. 1597-1612, 2013, doi: 10.1109/TSG.2013.2249541.

[35] J. Lu, S. Golestan, M. Savaghebi, J. C. Vasquez, J. M. Guerrero, and A. Marzabal, "An Enhanced State Observer for DC-Link Voltage Control of Three-Phase AC/DC Converters," *Ieee T Power Electr,* vol. 33, no. 2, pp. 936-942, 2018, doi: 10.1109/TPEL.2017.2726110.

[36] H. Wang *et al.*, "Continuous Fast Nonsingular Terminal Sliding Mode Control of Automotive Electronic Throttle Systems Using Finite-Time Exact Observer," *Ieee T Ind Electron,* vol. 65, no. 9, pp. 7160-7172, 2018, doi: 10.1109/TIE.2018.2795591.

[37] J. Sun, J. Yang, W. X. Zheng, and S. Li, "GPIO-Based Robust Control of Nonlinear Uncertain Systems Under Time-Varying Disturbance With Application to DC–DC Converter," *IEEE Transactions on Circuits and Systems II: Express Briefs,* vol. 63, no. 11, pp. 1074-1078, 2016, doi: 10.1109/TCSII.2016.2548298.

[38] R. Yang, L. Li, M. Wang, and C. Zhang, "Force Ripple Compensation and Robust Predictive Current Control of PMLSM Using Augmented Generalized Proportional Integral Observer," *IEEE Journal of Emerging and Selected Topics in Power Electronics,* pp. 1-1, 2019, doi: 10.1109/jestpe.2019.2938268.

[39] J. Wang, F. Wang, G. Wang, S. Li, and L. Yu, "Generalized Proportional Integral Observer Based Robust Finite Control Set Predictive Current Control for Induction Motor Systems With Time-Varying Disturbances," *Ieee T Ind Inform,* vol. 14, no. 9, pp. 4159-4168, 2018, doi: 10.1109/TII.2018.2818153.

[40] H. Sun, C. Dai, and S. Li, "Composite control of fuel quantity actuator system for diesel engines via backstepping control technique and generalised proportional integral observer," *IET Control Theory & Applications,* vol. 14, no. 4, pp. 605-613, 2020, doi: 10.1049/iet-cta.2019.0559.

[41] A. Yazdani and R. Iravani, "An accurate model for the DC-side voltage control of the neutral point diode clamped converter," *Power Delivery, IEEE Transactions on,* vol. 21, no. 1, pp. 185-193, 2006, doi: 10.1109/TPWRD.2005.852342.

[42] J. D. P. G.F.Franklin, and M.Workman, *Digital Control of Dynamic System,* . Addison Wesley Longman.Inc, 1998.

[43] C. E. Y Shtessel, L.Fridman, A. Levant, *Sliding mode control and observation*. New York USA: Springer, 2014.

[44] S. Kamran, H. Lennart, N. Hans-Peter, N. Staffan, and T. Remus, "Design, Control and Application of Modular Multilevel Converters for HVDC Transmission Systems," Wiley-IEEE Press, 2016, p. 416.

[45] F. d. Bosio, L. A. d. S. Ribeiro, F. D. Freijedo, M. Pastorelli, and J. M. Guerrero, "Discrete-Time Domain Modeling of Voltage Source Inverters in Standalone Applications: Enhancement of Regulators Performance by Means of Smith Predictor," *Ieee T Power Electr,* vol. 32, no. 10, pp. 8100-8114, 2017, doi: 10.1109/TPEL.2016.2632527.

[46] L. Harnefors, K. Pietilainen, and L. Gertmar, "Torque-maximizing field-weakening control: design, analysis, and parameter selection," *Ieee T Ind Electron,* vol. 48, no. 1, pp. 161-168, 2001, doi: 10.1109/41.904576.

Jinghang Lu (S'14-M'18) received the B.Sc. degree in electrical engineering from Harbin Institute of Technology, China, in 2009, two M.Sc. degrees both in electrical engineering from Harbin Institute of Technology, China, in 2011, and University of Alberta, Canada, in 2014, respectively, and the Ph.D. degree in Power Electronics from Aalborg University, Aalborg, Denmark, in 2018. From 2018 to 2019, He was a Research Fellow in Nanyang Technological University, Singapore. Currently, he is an Assistant Professor with Harbin Institute of Technology (Shenzhen), Shenzhen, China.

His research interests include uninterruptible power supply, microgrid, and control of power converters.

Mehdi Savaghebi (S'06-M'15-SM'15) was born in Karaj, Iran, in 1983. He received the B.Sc. degree from University of Tehran, Iran, in 2004 and the M.Sc. and Ph.D. degrees with highest honors from Iran University of Science and Technology, Tehran, Iran in 2006 and 2012, respectively, all in Electrical Engineering. From 2007 to 2014, he was a Lecturer in Electrical Engineering Department, Karaj Branch, Islamic Azad University. In 2010, he was a visiting Ph.D. Student with the Department of Energy Technology, Aalborg University, Aalborg, Denmark and with the Department of Automatic Control Systems and Computer Engineering, Technical University of Catalonia, Barcelona, Spain.

From 2014 to 2017, he was a Postdoc Fellow in the Department of Energy Technology, Aalborg University where he was an Associate Professor for 2017-2018. Currently, he is an Associate Professor with Electrical Engineering Section, the Mads Clausen Institute, University of Southern Denmark, Odense, Denmark.

His main research interests include distributed generation systems, microgrids, power quality and protection of electrical systems, UPS and smart metering. Dr. Savaghebi was a Guest Editor of Special Issue on Power Quality in Smart Grids, IEEE Transactions on Smart Grid and also a member of Task Force on Microgrid Stability Analysis and Modeling, IEEE Power and Energy Society. He is an Associate Editor of IEEE Access, a member of Technical Committee of Renewable Energy Systems, IEEE Industrial Electronics Society as well as Vice-Chair of sub-committee on Smart Buildings, IEEE Power and Energy Society.

Amer M.Y.M. Ghias (S'10–M'14) received the B. Sc. degree in electrical engineering from Saint Cloud State University, USA, in 2001, the M. Eng. degree in telecommunications from University of Limerick, Ireland, in 2006, and the Ph.D. degree in electrical engineering from the University of New South Wales (UNSW), Australia, in 2014. From February 2002 to July 2009, he had held various positions such as, Electrical Engineer, Project Engineer, and Project Manager, while working with the top companies in Kuwait. He has worked at UNSW, Australia (2014-2015) and the University of Sharjah, U.A.E (2015-2018). He is currently an assistant professor of the School of Electrical and Electronics Engineering, Nanyang Technological University, Singapore. His research interests include model predictive control of power electronics converter, hybrid energy storage, fault-tolerant converter, modulations and voltage balancing techniques for multilevel converter, flexible AC transmissions and high voltage DC current.

Xiaochao Hou received the B.S. and M.S. degrees from the School of Information Science and Engineering, Central South University, Changsha, China, in 2014 and 2017, respectively, where he is currently working toward Ph.D. degree in power electronics and power transmission. From 2018 to 2019 he is a joint Ph.D. student supported by the China Scholarship Council with the School of Electrical and Electronic Engineering of Nanyang Technological University. His research interests include renewable energy systems, distributed micro-grid, and power-electronic enabled power network.

Josep M. Guerrero (S'01-M'04-SM'08-FM'15) received the B.S. degree in telecommunications engineering, the M.S. degree in electronics engineering, and the Ph.D. degree in power electronics from the Technical University of Catalonia, Barcelona, in 1997, 2000 and 2003, respectively. Since 2011, he has been a Full Professor with the Department of Energy Technology, Aalborg University, Denmark, where he is responsible for the Microgrid Research Program (www.microgrids.et.aau.dk). From 2014 he is chair Professor in Shandong University; from 2015 he is a distinguished guest Professor in Hunan University; and from 2016 he is a visiting professor fellow at Aston University, UK, and a guest Professor at the Nanjing University of Posts and Telecommunications.

His research interests is oriented to different microgrid aspects, including power electronics, distributed energy-storage systems, hierarchical and cooperative control, energy management systems, smart metering and the internet of things for AC/DC microgrid clusters and islanded minigrids; recently specially focused on maritime microgrids for electrical ships, vessels, ferries and seaports. Prof. Guerrero is an Associate Editor for a number of IEEE TRANSACTIONS. He has published more than 450 journal papers in the fields of microgrids and renewable energy systems, which are cited more than 30,000 times. He received the best paper award of the IEEE Transactions on Energy Conversion for the period 2014-2015, and the best paper prize of IEEE-PES in 2015. As well, he received the best paper award of the Journal of Power Electronics in 2016. During five consecutive years, from 2014 to 2018, he was awarded by Thomson Reuters as Highly Cited Researcher. In 2015 he was elevated as IEEE Fellow for his contributions on "distributed power systems and microgrids."